Radioactive Decay

Example – atoms in a jar

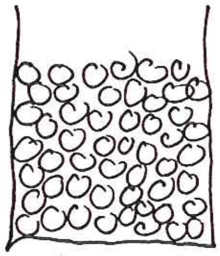

P_0 = initial number of parent atoms at time $t = 0$

Every atom has an equal probability to decay:

$$\boxed{p = \text{probability of decay / unit time}}$$

In a large sample of atoms:

$$\boxed{p = \frac{\text{fraction that decay}}{\text{unit time}}}$$

← units of p (yr^{-1})

Say the unit time is one year.
The number of atoms left in the jar at subsequent times is

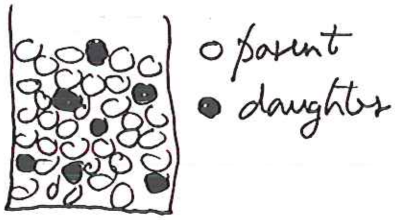

$t = 0$: P_0

$t = 1$: $P_0(1-p) = P_1$

$t = 2$: $P_1(1-p) = P_0(1-p)^2 = P_2$

$\vdots$

$$\boxed{\text{In general} \quad P_t = P_0(1-p)^t}$$

Rewrite as $P_t = P_0 \, e^{t \ln(1-p)}$

Define the <u>decay constant</u>:

$$\boxed{\lambda = -\ln(1-p) \approx p, \text{ for small } p}$$

Law of radioactive decay:

$$\boxed{P_t = P_0 \, e^{-\lambda t}} \leftarrow \text{exponential decay}$$

Number of daughter atoms:

$$\boxed{D_t = P_0 - P_t = P_0 \left(1 - e^{-\lambda t}\right)}$$

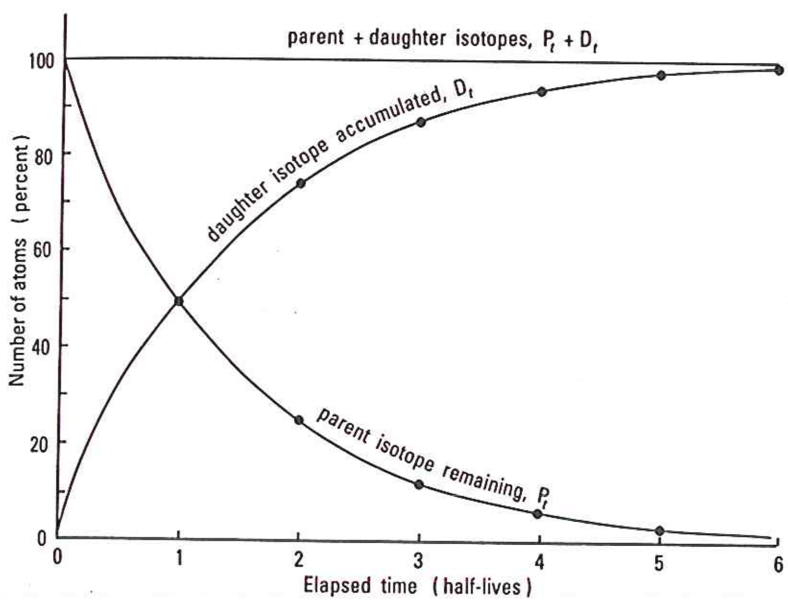

Fig. 3.2. Decay of a radioactive parent isotope and the corresponding accumulation of its daughter isotope. In a closed system, the sum of the parent and daughter isotopes at any time equals the original amount of the parent isotope.

<u>Half-life</u>: time required for half of initial population to decay

$$\frac{1}{2} P_0 = P_0 e^{-\lambda \tau_{1/2}}$$

$$\lambda \tau_{1/2} = -\ln\left(\frac{1}{2}\right) = \ln 2$$

$$\boxed{\tau_{1/2} = \frac{\ln 2}{\lambda} = \frac{0.693}{\lambda}}$$

<u>Radiometric age determination</u>:

$$P_t = P_0 e^{-\lambda t} \qquad \boxed{t = \frac{1}{\lambda} \ln\left(\frac{P_0}{P_t}\right)}$$

need to know number P_0 of parent atoms at $t=0$

Okay for ^{14}C but not for most other applications

$$P_t = P_0 e^{-\lambda t} \Rightarrow P_0 = P_t e^{\lambda t}$$

$$D_t = P_0 (1 - e^{-\lambda t}) = P_t (e^{\lambda t} - 1)$$

$$e^{\lambda t} = \frac{D_t}{P_t} + 1 \qquad \boxed{t = \frac{1}{\lambda} \ln\left(\frac{D_t}{P_t} + 1\right)}$$

in terms of amounts P_t, D_t of parent and daughter <u>now</u>

More typically, the number of daughter atoms D_0 at time zero will <u>not</u> be zero

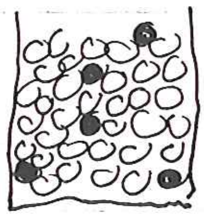

• $D_0 \neq 0$ at $t = 0$

In that case, $D_t = D_0 + P_0(1 - e^{-\lambda t})$

$$= D_0 + P_t(e^{\lambda t} - 1)$$

$$\boxed{t = \frac{1}{\lambda} \ln\left(\frac{D_t - D_0}{P_t} + 1\right)}$$

← must correct for initial amount D_0 of daughter by subtraction

In practical applications:

- either D_0 is negligible, e.g. K–Ar method
- or knowledge of D_0 is finessed — <u>isochron</u> method

<u>^{14}C dating</u>: not used to date rocks or meteorites, only <u>organic remains</u>

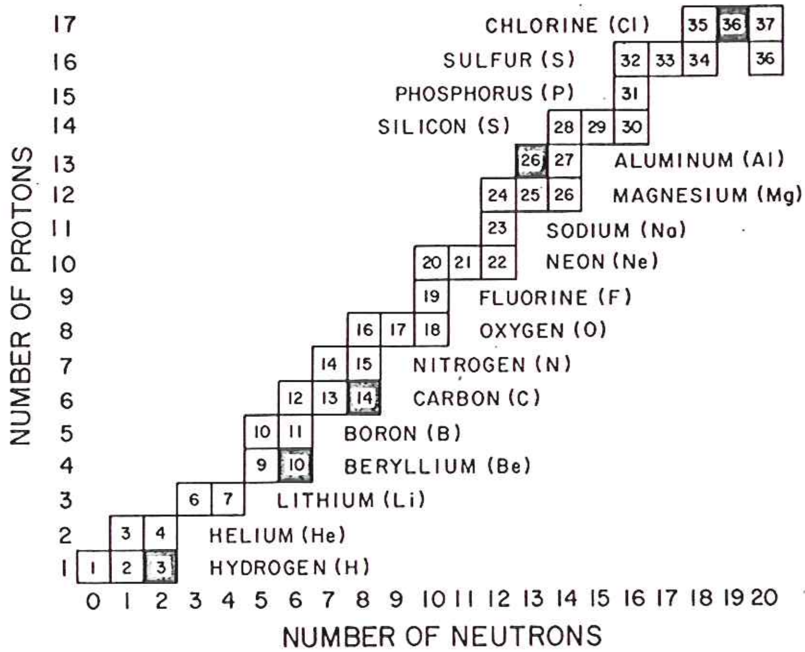

Figure 2-13. Chart of the nuclides: Shown in this series of diagrams are all the nuclides present in nature. The black squares represent radioactive isotopes.

Carbon abundances

^{12}C — 99% } stable
^{13}C — 1°

^{14}C only about 10^{-12}
unstable — decays to ^{14}N by β decay

Half-life:

$\tau_{1/2} = 5730 \pm 30$ years

Only present because produced by cosmic ray bombardment (fast neutron capture)

$n + {}^{14}N \rightarrow {}^{14}C + p^+ + e^-$

in upper atmosphere

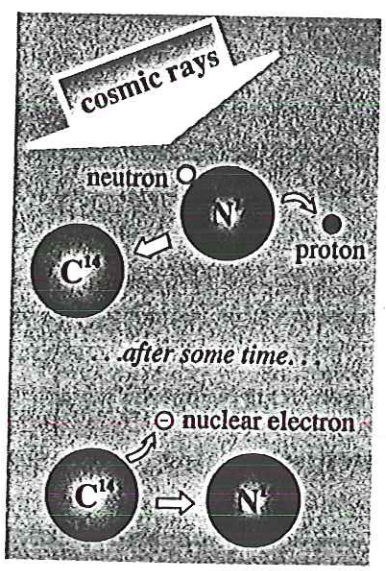

Figure 5.2. Production of ^{14}C from nitrogen and cosmic rays, and its decay. After Cloud (1988, p. 84).

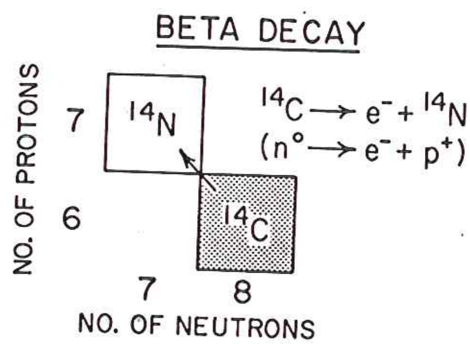

Atmosphere is ~ 80% nitrogen

^{14}N — 99.6%
^{15}N — 0.4%

Atmospheric ^{14}C is quasi-steady state:

cosmic ray production ⇒ $\boxed{^{14}C \text{ in atmosphere}}$ ⇒ radioactive decay

$$\left({}^{14}C\right)_{\substack{\text{sample of}\\ \text{dead organic}\\ \text{matter}}} = \left({}^{14}C\right)_{\text{atmosphere}}\, e^{-\lambda t}$$

Divide by $\left({}^{12}C\right)_{\text{atomosphere}} = \left({}^{12}C\right)_{\text{sample}}$:

$$\left(\frac{{}^{14}C}{{}^{12}C}\right)_{\text{sample}} = \left(\frac{{}^{14}C}{{}^{12}C}\right)_{\text{atmosphere}} e^{-\lambda t}$$

$$\boxed{t = \frac{1}{\lambda} \ln \frac{\left({}^{14}C/{}^{12}C\right)_{\text{atmosphere}}}{\left({}^{14}C/{}^{12}C\right)_{\text{sample}}}} \qquad \boxed{\lambda = \frac{0.693}{5730\ \text{yr}} = 1.21 \cdot 10^{-4}\ \text{yr}^{-1}}$$

For accurate dates need to correct for non-uniform cosmic-ray production rate

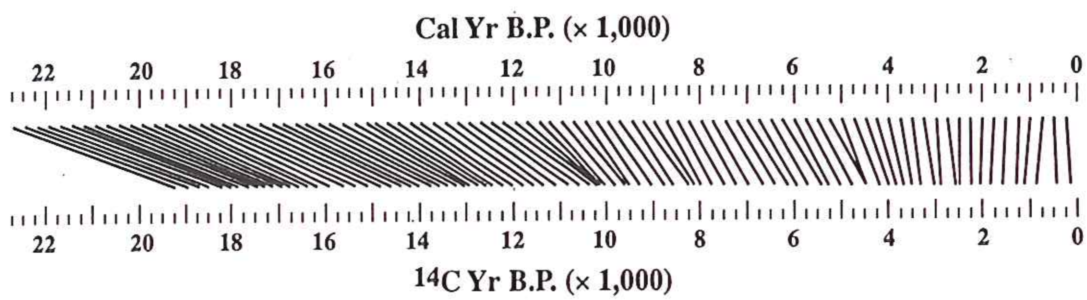

Figure 5.3. Relationship between actual age of a sample (cal yr before present; B.P.) and the age from carbon-14 dating (^{14}C yr B.P.). Both axes are in units of thousands of years, and so, the figure goes back to 22,000 years ago. From Bartlein et al. (1995) by permission of Academic Press.

FIGURE 13.4 Carbon-14 age as a function of dendrochronological age for the past 1000 yr (from Stuiver, 1982). Note deviations from concordance line that have a 100-200-yr period.

accurate calibration for past 1000yrs — bristlecone pine tree rings

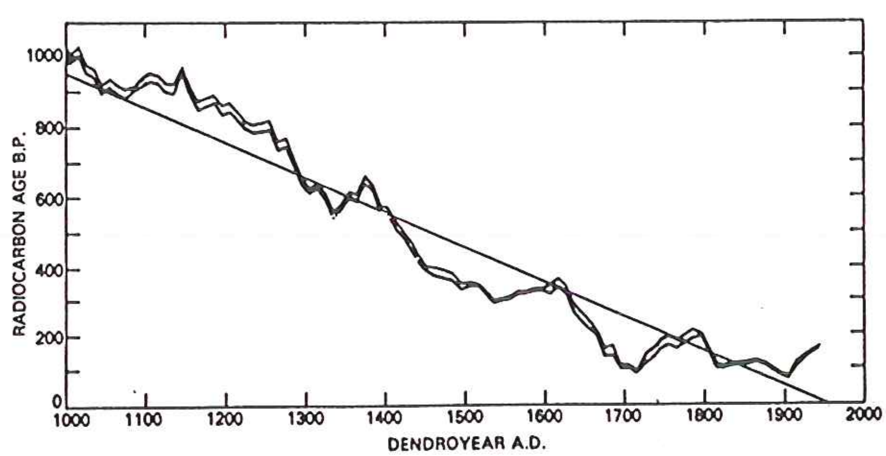

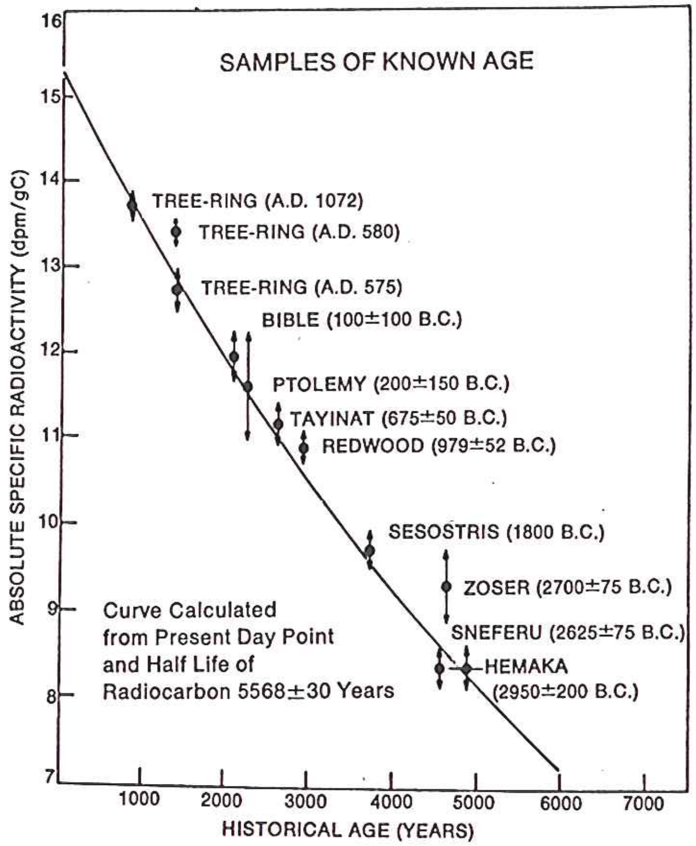

FIG. 10. Willard Libby's check of the basic soundness of the radiocarbon method. Observed radioactivities of historically dated samples are plotted against the curve, which shows the predicted values. The good agreement was confirmation of the validity of the method. (*After W. F. Libby*)

Original implementation by Libby used a geiger counter to measure $({}^{14}C)_{sample}$ and $({}^{14}C)_{atmosphere}$

Disadvantage – large amounts and long counting times needed for older samples

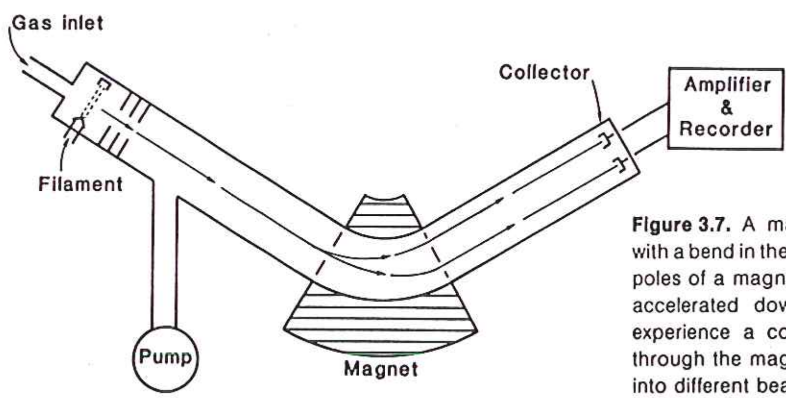

Figure 3.7. A mass spectrometer is a tube with a bend in the middle between the opposite poles of a magnet. Atomic or molecular ions accelerated downtube by a voltage drop experience a constant force while passing through the magnet and are thus separated into different beams according to mass.

Non-archaeological application of ${}^{14}C$ dating:
Paleoseismology – times of occurrence of past earthquakes on the San Andreas Fault – Kerry Sieh – Caltech

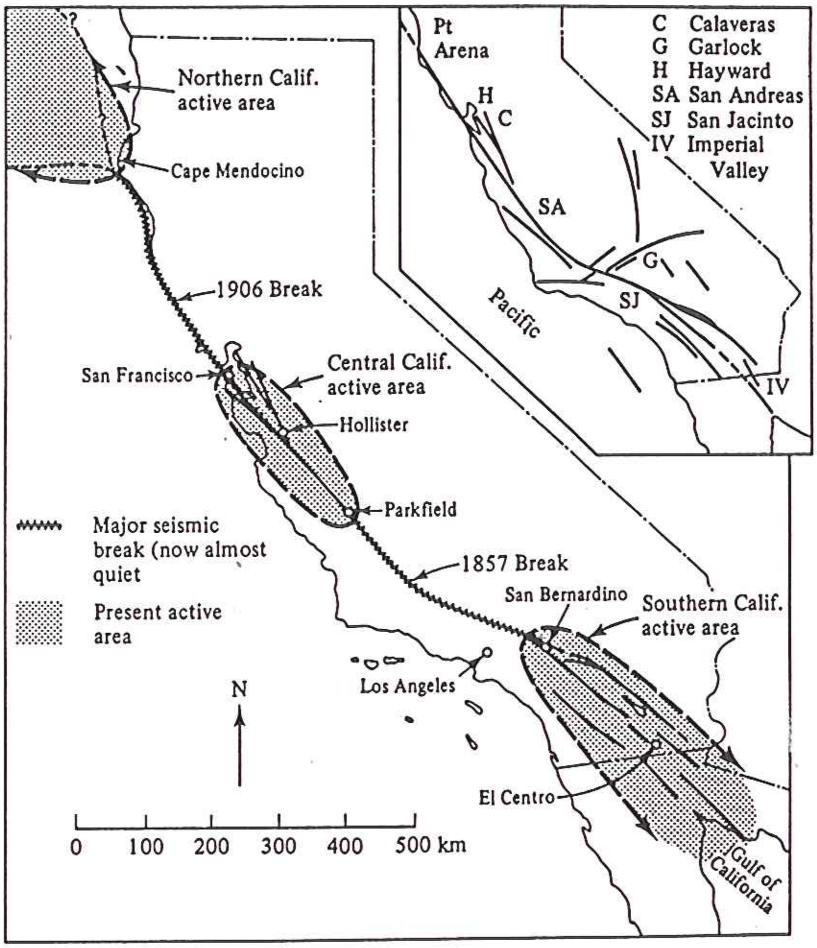

Fig. 7.1. Areas of contrasting seismic behaviour along the San Andreas fault zone. in California. (After Allen, 1968.)

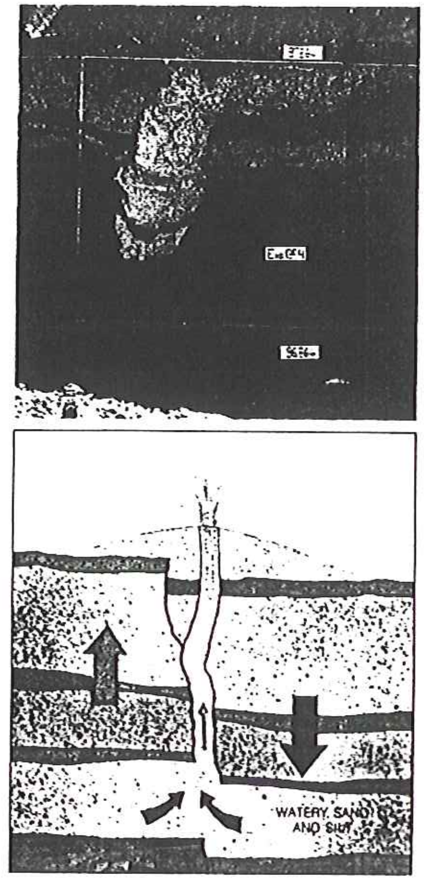

Remnants of a sandblow—a spouting of sand and water caused by moderate to severe earthquakes—can be seen in the photograph of a cross section of an old California stream bed that was rocked by a quake around 1700. Sandblows occur, as illustrated in the drawing at bottom, when a layer of subsoil takes on liquid characteristics during tremors. Pressure drives the watery sand and silt up through a fissure, leaving a mound of sediment on the surface that geologists can use to identify and date the earthquake.

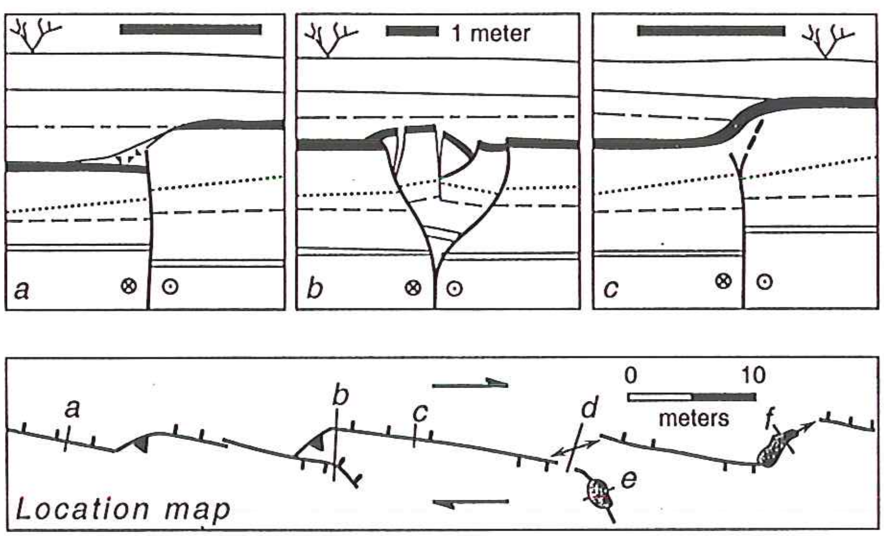

Figure 8–58. These idealized cross sections across strike-slip faults show various kinds of evidence for paleoseismic events. Top of solid black bed is the event horizon. Shaded horizontal bars are 1 meter long. Lines with arrows on location map indicate crests of anticlinal folds. Mismatches of strata across some of the faults is an indication of strike-slip motion.

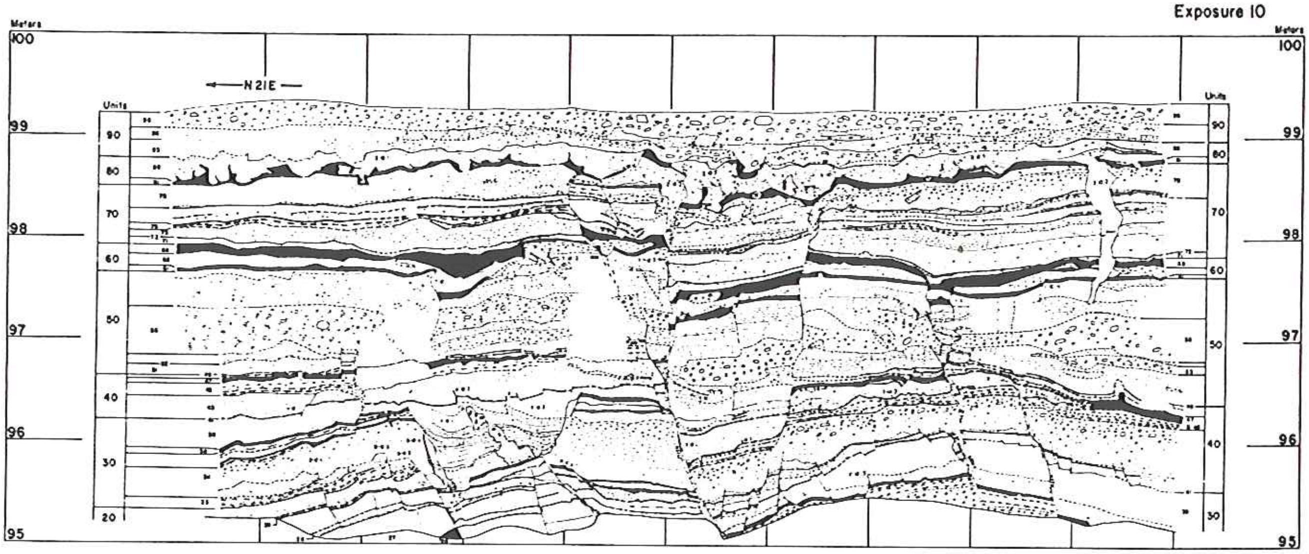

Figure 8–60. Map of trench wall shows evidence for eight earthquakes on San Andreas fault between about A.D. 750 and 1857. Grid spacing is one meter. For large-scale reproduction, see Sieh (1978a).

Mean recurrence interval on Mojave segment of San Andreas 130 years

Evidence for clustering in time.

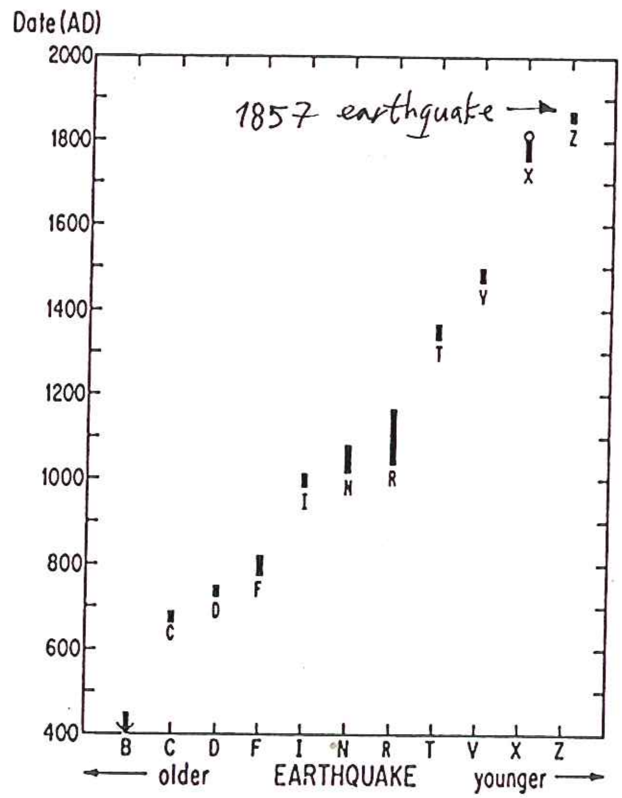

Fig. 6. New estimates of the dates for earthquakes recorded in the sediments at Pallett Creek. Bars give 95% confidence intervals. Open circle on bar of event X indicates preferred date of A.D. 1812.

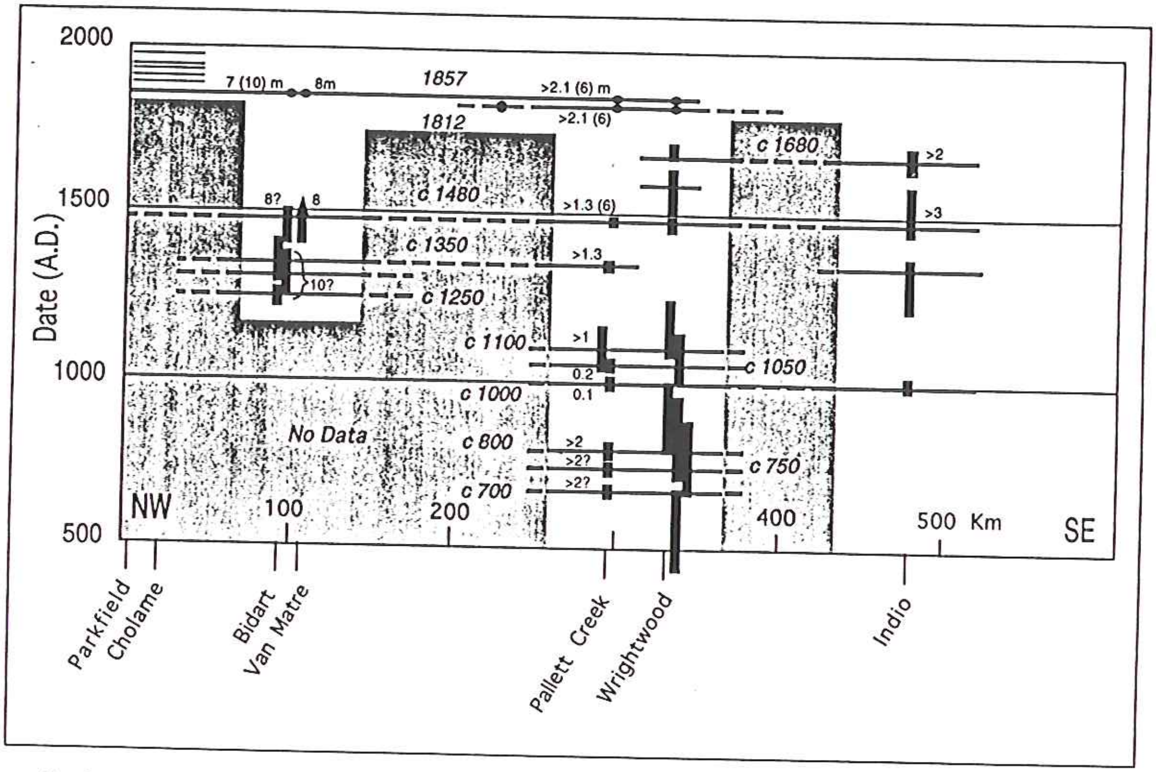

Figure 8–65. This history of large ruptures along the San Andreas fault is based upon data from several paleoseismic sites. Thick horizontal lines represent rupture lengths, based upon proposed correlations between sites. Dextral offsets are indicated (in meters) where available. Offsets in parentheses represent broad-aperture values, whereas others represent offsets measured in 3D excavations only within the fault zone. Values queried where more speculative. Though woefully incomplete, the currently available record demonstrates the clustered nature of earthquake occurrence along the fault and the inappropriateness of the characteristic- or uniform-earthquake model for the San Andreas fault. Modified from Grant and Sieh (1994), with additions from Sieh (1984), Salyards et al. (1992) and other sources.

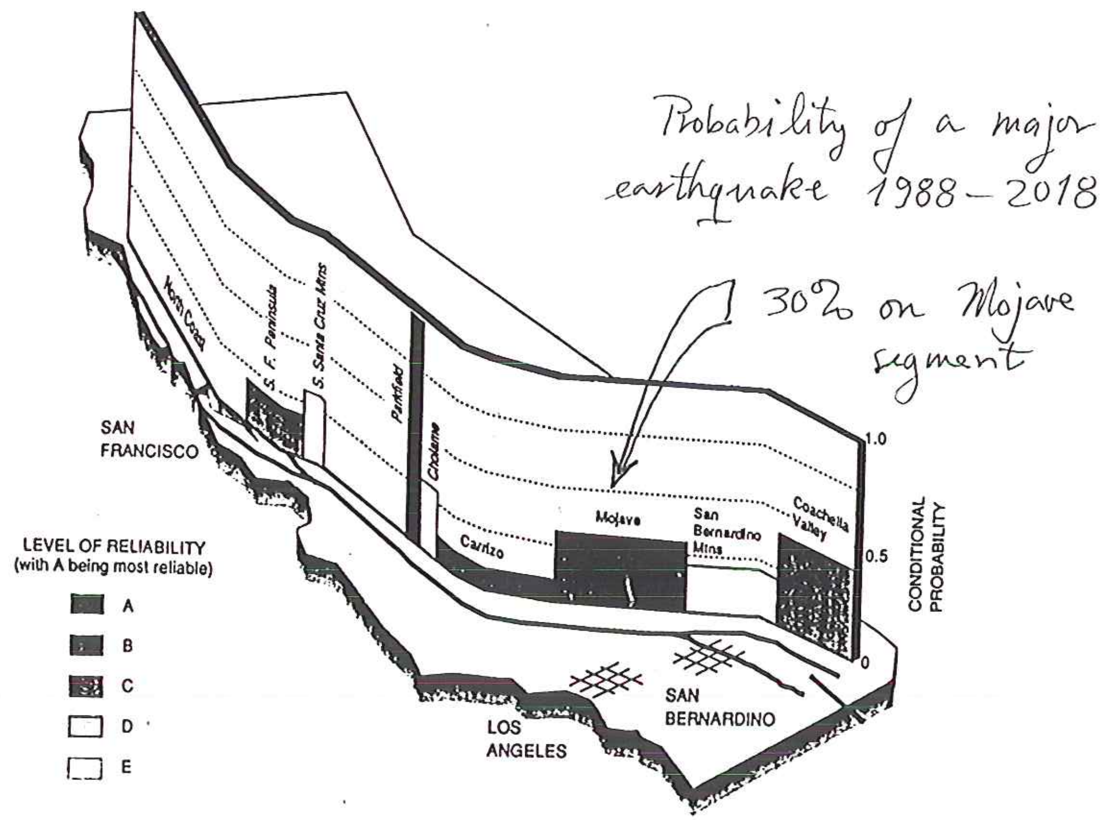

FIGURE 11.B3.2 The conditional probability of major earthquakes along different segments of the San Andreas fault. The probability illustrated is for the time interval 1988–2018. (From Agnew *et al.*, 1988).